

# Analysis of spinal motion and loads during frontal impacts. Comparison between PMHS and ATD

Francisco J. Lopez-Valdes<sup>1,2</sup>, Anthony Lau<sup>1</sup>, John Lamp<sup>1</sup>, Patrick Riley<sup>1</sup>, David J. Lessley<sup>1</sup>,  
Andrew Damon<sup>1</sup>, Matthew Kindig<sup>1</sup>, Richard Kent<sup>1</sup>  
<sup>1</sup>University of Virginia, <sup>2</sup>ECIP- Universidad de Navarra

Sriram Balasubramanian, Thomas Seacrist, Matthew R. Maltese, Kristy B. Arbogast  
The Children's Hospital of Philadelphia

Kazuo Higuchi, Hiro Tanji  
Takata Corp.

---

**ABSTRACT** – Quantifying the kinematics of the human spine during a frontal impact is a challenge due to the multi-degree-of-freedom structure of the vertebral column. This paper reports on a series of six frontal impact sled tests performed on three Post Mortem Human Surrogates (PMHS). Each subject was exposed first to a low-speed, non-injurious frontal impact (9 km/h) and then to a high-speed one (40 km/h). Five additional tests were performed using the Hybrid III 50<sup>th</sup> percentile male ATD for comparison with the PMHS. A 3D motion capture system was used to record the 6-degree-of-freedom motion of body segments (head, T1, T8, L2, L4 and pelvis). The 3D trajectories of individual bony structures in the PMHS were determined using bone-mounted marker arrays, thus avoiding skin-attached markers and their potential measurement artifacts. The PMHS spines showed different behavior between low and high speed. While at low speed the head and upper spinal segments lagged the lower portion of the spine and pelvis in reaching their maximum forward displacement (time for maximum forward head excursion was 254.3±31.9 ms and 140.3±9 ms for the pelvis), these differences were minimal at high speed (127±2.6 ms for the head vs. 116.7±3.5 ms for the pelvis). The ATD did not exhibit this speed-dependant behavior. Furthermore, the ATD's forward displacements were consistently less than those exhibited by the PMHS, regardless of the speed. Neck loads at the atlanto-occipital joint were estimated for the PMHS using inverse dynamics techniques and compared to those measured in the ATD. It was found that the axial and shear forces and the flexion moment at the upper neck of the PMHS were higher than those measured in the ATD.

---

## INTRODUCTION

Spinal kinematics dictates the position, speed and attitude of the head during a frontal impact. The assessment and prevention of traumatic brain and skull injuries will benefit from accurate kinematic data that help to understand the three dimensional (3D) displacement of the head throughout the impact. Several studies have reported that current Anthropomorphic Test Devices (ATD) can correctly predict the magnitude of the maximum forward head excursion though they are unable to replicate the exact trajectory followed by the head (Sherwood et al., 2003; Lopez-Valdes et al., 2009). Other studies have highlighted the differences found comparing ATD spinal kinematics with those of humans (Shaw et al., 2001). The discrepancy between ATD and Post Mortem Human Surrogates PMHS has been attributed to the stiffness of the ATD spine in comparison to the flexible multi-segment arrangement of the human one. Sherwood et al. (2003) suggested that the stiff spine of pediatric ATD

(obtained by scaling adult ATD) causes the dummy neck to sustain unrealistically high forces and moments and eventually to exceed the proposed injury thresholds in a non-biofidelic manner. The analysis of the biofidelity of the Hybrid III 50<sup>th</sup> percentile neck and the associated injury criteria was originally performed in the late 1960s and early 1970s (Mertz and Patrick, 1971; Culver et al., 1972) based on volunteer and cadaveric studies. Subsequent studies have identified lack of biofidelity under some loading environments (Seeman et al., 1986; Yoganandan et al., 1989). In the case of a pediatric ATD, it has been reported that the published thresholds for the cervical spine injury metrics (Nij and neck tension) as well as the Head Injury Criterion (HIC) are often exceeded in frontal sled and full vehicle impact tests (Menon et al., 2003; Sherwood et al., 2003; Malott et al., 2004). These results are at odds with studies reporting the rarity of pediatric neck injuries in the field (Durbin, 2002; Arbogast et al., 2002; Zuckerman et al., 2004).

The measurement of spinal kinematics *in situ* presents significant experimental challenges, deriving primarily from the lack of sight lines to the vertebral column in an intact PMHS. Point tracking of surface markers has been used in the past to estimate two-dimensional (2D) or even 3D motion using high speed video cameras, but the effect of skin motion during the test creates an unquantifiable error between the tracked points and the actual motion of the spine. In the present study, a 3D motion capture system was used and arrays of orthogonal markers were rigidly attached to the vertebral bodies at different spinal levels, allowing for an accurate description of the kinematics of the head and the internal structures of the spine during the impact.

A total of six sled tests was performed on three PMHS with an anthropometry close to a 50<sup>th</sup> percentile male. Each subject was tested twice: first, in a non-injurious impact at low speed (9 km/h) and then in a high-speed impact (40 km/h). A series of five ATD tests using the Hybrid III 50<sup>th</sup> percentile male was also done in the same conditions used for the PMHS. The current study has two primary objectives:

- To describe the *in situ* pelvic, spinal and head kinematics of PMHS during a simulated frontal impact in the sagittal plane at two different speeds (9 km/h and 40 km/h) and compare with those of ATD.
- To evaluate whether the ATD accurately predicted the upper neck (atlanto-occipital joint) forces and moments experienced by PMHS in a frontal impact.

## METHODS

### Test setup

A total of 11 tests were analyzed in this study, five involving the Hybrid III 50<sup>th</sup> percentile and six involving three PMHS. Both ATD and PMHS were exposed first to a low-speed, non-injurious deceleration pulse and then to a high-speed pulse (see Figure 1). The test matrix is shown in Table 1. While the goal of the low speed tests was to compare with the results of a study performed with volunteers (Arbogast et al., 2009), at high speed, the test was design to maximize spinal flexion. Therefore a rigid knee bolster was used to restraint the forward pelvic motion of the occupants.

The test fixture was designed to provide a reasonable approximation of frontal impact kinematics of a restrained occupant in a vehicle, while providing repeatable and reproducible conditions and line-of-

sight for the motion capture system (Shaw et al. 2009).

Table 1. Test matrix.

	Low speed	High speed
Hybrid III 50 <sup>th</sup> (test number)	1395, 1396	1443, 1444, 1445
PMHS (test number)	1397, 1401, 1404	1398, 1402, 1405
Knee bolster	No	Yes
Test speed	9 km/h	40 km/h

Occupants were restrained by a conventional 3-point belt equipped with a retractor. Initial positioning of the subjects and belt geometry were chosen to allow comparing with the results of the volunteer study (Arbogast et al., 2009) and representing real world geometry. Test subjects were positioned on a flat rigid seat with the torso and head being supported by a set of cables that were adjustable in height and tension.

Torso angle (as measured between the spinous process of T1, the position of the greater trochanter and the horizontal) was set (nominally) to 110 degrees in the cadavers. In the case of ATD, torso angle was defined as the angle between the shoulder and the H-point and it was set at 110 degrees initially. The angle between the femur and the tibia at the knee joint was also set (nominally) to 110 degrees, both in the ATD and the PMHS. Figure 2 shows this fixture and the initial position of one of the PMHS.

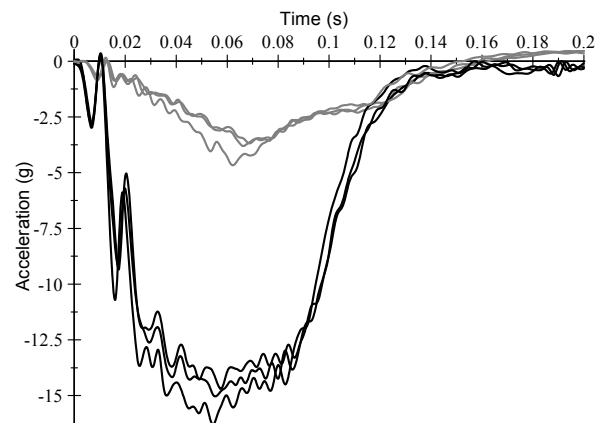


Figure 1. Low speed (gray) and high speed (black) crash pulses used in the study for the PMHS.

### Motion capture system

Kinematic data were obtained using a 16-camera Vicon MX<sup>TM</sup> motion capture system operating at 1000 Hz. The cameras tracked the motion of

spherical retroreflective targets within the cameras' collective viewing volume. A calibration procedure, performed prior to testing each subject, estimated the optical characteristics of each camera and established its position and orientation in a reference coordinate system. With this information a photogrammetric algorithm within the Vicon Nexus software package reconstructed the 3D position of each target for each video sample increment from the multiple 2D camera images.

### PMHS information

The three PMHS included in this study were screened before testing and confirmed free of blood infectious diseases (HIV, Hepatitis B and C). Absence of any other pathology that could influence injury occurrence was also confirmed via high-resolution computed tomography (CT) scans. Anthropometric characteristics of the PMHS can be found in Table 2. PMHS were chosen to be as close as possible to a 50<sup>th</sup> percentile male. The experiments were performed according to the Protocol for the Handling of Biological Material (Center for Applied Biomechanics, 2006) and approved by the University of Virginia – Center for Applied Biomechanics Oversight Committee.

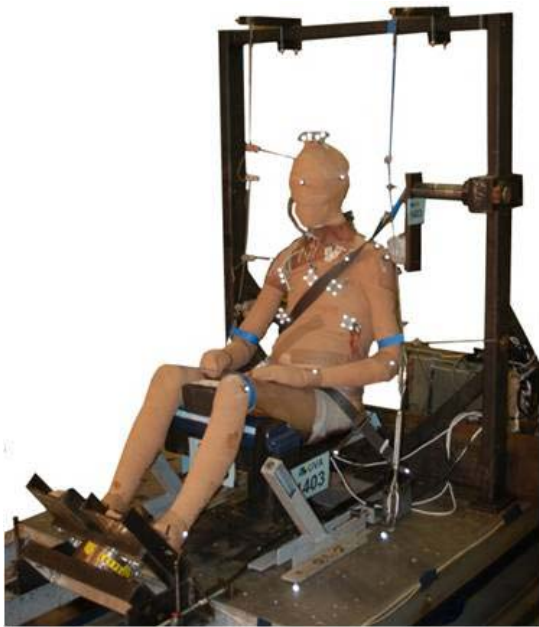


Figure 2. Test fixture and PMHS initial position

After testing, PMHS were subjected to a CT scan examined by a radiologist followed by an autopsy. Injuries are reported according to AIS 2005 (AAAM, 2005)

*PMHS head mass, center of gravity and moment of inertia estimation.* The total mass, center of gravity (CG), and moments of inertia (MOI) of the specimens' heads were found using computed tomography (CT) images. Methodologies were taken from previous research (Damon, 2009). Head mass was found by measuring the volume of bone and soft tissue in Voxar 3D (Barco, N.V.; Bruges, Belgium) and assigning density values to these regions. Soft tissue was assumed to have the same density as water (1 g cm<sup>-3</sup>), and bone density (1.92 g cm<sup>-3</sup>) was chosen based on published research (O'Flaherty, 1991).

Table 2. PMHS information

	PMHS 393	PMHS 462	PMHS 422
Test number	1397, 1398	1401, 1402	1404, 1405
Age (years)	59	69	60
Gender	Female	Male	Male
Cause of death	Renal failure	Kidney failure	Renal failure
Stature (cm)	167	178	191
Weight (kg)	80	84	81
Seated height (cm)	93	92	93

To measure the CG and MOI of the head, an anatomical coordinate system was established based on the Frankfort plane. Using the orbital notches and the external auditory meati, the CT images were oriented into the Frankfort plane. Next, each voxel of the CT image was assigned a mass based on thresholding that determined if the voxel was soft tissue, bone, or air. The center of gravity of the head, CG, was then found using Eq. 1, where  $mass_{head}$  is the total mass of the head,  $M_n$  is the moment contribution of each voxel about an arbitrary axis of rotation, and  $v$  is the total number of voxels in the scan.

$$CG = \frac{\sum_{n=1}^v M_n}{mass_{head}} \quad (1)$$

Once the  $CG_{head}$  was located, the MOI was found by summing the moment of inertia of each voxel about the CG. The CG and MOI calculations were repeated for each coordinate axis.

### Instrumentation

*Reflective markers.* Orthogonal arrays of four markers were attached to the superior aspect of the skull, right acromion, T1, T8, L2, L4, pelvis, 4<sup>th</sup> and 8<sup>th</sup> ribs bilaterally and sternum. These arrays allow

the 6 DOF reconstruction of the motion of each structure. The method first obtains the transformation matrix between the coordinate system defined by the array of markers and the local coordinate system of the concerned bone ( $T_{ArrayCS}^{BoneCS}$ ). Then, this matrix can be combined with the transformation matrix between the coordinate system of the array of markers and any other coordinate system defined within the VICON environment ( $T_{GlobalCS}^{ArrayCS}$ ). The combination of these two matrices makes possible obtaining the position and orientation of a local coordinate system with respect a different coordinate system according to equation 2 (Kinzel et al., 1972).

$$T_{GlobalCS}^{BoneCS} = T_{ArrayCS}^{BoneCS} \cdot T_{GlobalCS}^{ArrayCS} \quad (2)$$

In this study, a coordinate system attached to the test fixture and oriented according to the SAE J211 criterion was chosen. Therefore, the trajectories discussed in the paper are the trajectories of the relevant bone with respect to the buck and expressed in the SAE J211 coordinate system. The creation of each bony local coordinate system as well as detailed information on the process of the data is described by Shaw et al. (2009).

Clusters of four retroreflective markers were secured to analogous components on the Hybrid III dummy (head, spine and pelvis). In this case, the transformation from the marker cluster geometry to the structure was derived from the known mount hardware geometry, in some cases augmented by measurements made with a precision kinematic linkage (FARO). In addition to the marker clusters, individual markers were used to determine the position (3DOF) of points of interest.

*Other (non-optical) instrumentation.* Tri-axial accelerometers (Endevco model 7264B) were mounted on head, T1, T8, L2 and pelvis. Tri-axial angular rate sensors (DTS model ARS-12k) were also used on the head and T1. All these instruments were rigidly attached to the correspondent anatomical structure through mounting plates screwed into the bones. The relative position and orientation of these sensors with respect to the center of gravity of the bone was obtained using CT images, allowing for transformation between the local instrument coordinate system and the correspondent local anatomical system. A comprehensive description of cadaver preparation and sensor installation can be found in Shaw et al. (2009). Tension belt gages (Model 419-3.5 K, Eaton Lebow) were attached to three locations on the seatbelt (upper shoulder, inner

lap and outer lap portions). Load cells were used under the seat, in the knee bolster (when mounted) and under the feet support. Instrument data were collected using an onboard TDAS data acquisition system at 10,000 Hz.

### Determination of neck loads from inverse dynamics

Upper neck forces and moments ( $F_x$ ,  $F_z$ ,  $M_y$ ) were estimated for the PMHS using inverse dynamics. The reactions forces were resolved in a local coordinate system placed at the center of the occipital condyle junction and oriented parallel to the head anatomical coordinate system. This was considered to be analogous to the coordinate system of the upper neck load cell in the Hybrid III. The method was first applied by Mertz (1967) and recently used by Funk et al. (2009). The equations used to estimate the neck loads at the OC-C1 joint were the following:

$$F_x = m_{head} a_{CGx} - m_{head} g \sin \theta \quad (3)$$

$$F_z = m_{head} a_{CGz} - m_{head} g \cos \theta \quad (4)$$

$$M_y = -I_{head} \alpha - F_x r_z - F_z r_x - m_{head} g r_z \sin \theta - m_{head} g r_x \cos \theta \quad (5)$$

where  $a_{CGx}$  and  $a_{CGz}$  were the acceleration of the head CG with respect the local coordinate axis “x” and “z” respectively,  $\theta$  was the angle formed between the local “x” axis and the horizontal (global “X” axis) and was defined positive in the counter-clockwise direction. The value of the acceleration projected on the head anatomical system was obtained transforming the acceleration measured at the head plate to the head anatomical system (SAE convention) placed at the head CG using rigid body kinematics. First, the measurements obtain from the tri-axial accelerometers were transformed to an anatomical oriented coordinate system still placed at the mount location. Second, the acceleration at the head CG was calculated according to Equation 6 (Beer et al., 2004):

$$\underline{a}_{CG} = \underline{a}_{MOUNT} + \underline{\alpha} \times \underline{r} + \underline{\omega} \times (\underline{\omega} \times \underline{r}) \quad (6)$$

where  $\underline{r}$  is the vector connecting the origin of the mount and the head CG. Angular acceleration was obtained by differentiation of the angular speed measured by the angular rate sensors. The value of the angle  $\theta$  was calculated integrating the ARS measurements. Initial angle at  $t=0$  was obtained from the motion capture system. The other parameters involved in the equations corresponded to the

anthropometric characteristics of the subjects and their values are shown in Table 3. The relevant moment of inertia (MOI) for the inverse dynamic calculations is about the “y” local axis and  $r_x$ ,  $r_z$  are the components of the vector between the head CG and the center of the OC-C1 junction projected on the local “x” and “z” axes respectively.

Table 3 PMHS and Hybrid III 50<sup>th</sup> anthropometric head values used in the inverse dynamics calculations.

Subject	Head mass (kg)	MOI <sub>y</sub> (kg·m <sup>2</sup> )	r <sub>x</sub> (mm)	r <sub>z</sub> (mm)
393	4.54	0.0223	10.13	58.90
422	5.09	0.0290	12.98	60.00
462	4.90	0.0279	19.56	71.50
Hybrid III 50 <sup>th</sup>	4.40	0.0204	22.00	51.00

## RESULTS

### Spinal trajectories

Table 4 and Table 5 show the values and timing of the maximum forward excursion of the head, spine and pelvis obtained in the ATD and PMHS tests, respectively.

Table 4. Mean excursion of ATD head, spine and pelvis ( $\pm$  standard deviation). Low speed. X(mm), time (ms).

	X	t
Head	178.3 ( $\pm$ 2)	159 ( $\pm$ 0)
Spine	102 ( $\pm$ 1.8)	138.5 ( $\pm$ 6.4)
Pelvis	87.0 ( $\pm$ 0.5)	140.0 ( $\pm$ 9.9)

Table 5. Forward excursion of PMHS head, vertebrae and pelvis. Low speed. X(mm), time (ms).

	1397		1401		1404	
	X	t	X	t	X	t
Head	283.8	233	291.6	239	319.74	291
T1	211.0	223	203.7	200	217.3	207
T8	161.4	190	129.7	280	157.7	167
L2	95.78	162	80.40	154	108.4	148
L4	70.38	157	64.1	149	NA	NA
Pelvis	51.96	149	58.5	141	67.5	131

Peak forward excursion and timing of the event at high speed are shown in Tables 6 and 7 both for the ATD and the PMHS.

To illustrate the different nature of the trajectories followed by the ATD segments and the PMHS bony structures, the kinematic data from PMHS 393 is shown side by side to the trajectories followed by the ATD head, spine and pelvis in Figures 3 and 4.

Table 6. Mean excursion of ATD head, spine and pelvis ( $\pm$  standard deviation). High speed. X(mm), time (ms).

	X	t
Head	435.7 ( $\pm$ 11.6)	124.7 ( $\pm$ 1.15)
Spine	239.9 ( $\pm$ 0.9)	130 ( $\pm$ 2.6)
Pelvis	19.3 ( $\pm$ 0.3)	71.3 ( $\pm$ 4.2)

Table 7. Forward excursion of PMHS head, vertebrae and pelvis. High speed. X(mm), time (ms).

	1398		1402		1405	
	X	t	X	t	X	t
Head	493.8	126	572.2	125	525.4	130
T1	428.17	133	457.2	133	418.7	134
T8	385.7	132	346.4	117	327.7	128
L2	242.2	124	208.5	106	208.9	116
L4	168.9	120	148.7	104	NA	NA
Pelvis	104.38	120	67.51	117	64.85	113

Selected video captures corresponding to different times up to the time of maximum head forward excursion are included in Figure 5 to illustrate the kinematics of one of the subjects during a high speed test.

The trajectories corresponding to each bony structure are plotted in the XZ plane in Figure 6, showing the differences between low and high speed runs for each PMHS. Trajectories are plotted until the maximum head forward excursion is reached. The dashed lines connect intermediate positions of each segment every 50 ms. Lower segments of the spine and the pelvis exhibited a different behavior between the low and high speed tests. At low speed these structures were moving backward (rebounding) when the head reached its maximum forward excursion. Also, trajectories remained parallel between the different segments. In the high speed tests, the head, spine and pelvis moved more synchronously, reaching their peak forward excursion at about the same time. At this speed, the pelvis moved upwards compressing the lower lumbar section of the spine.

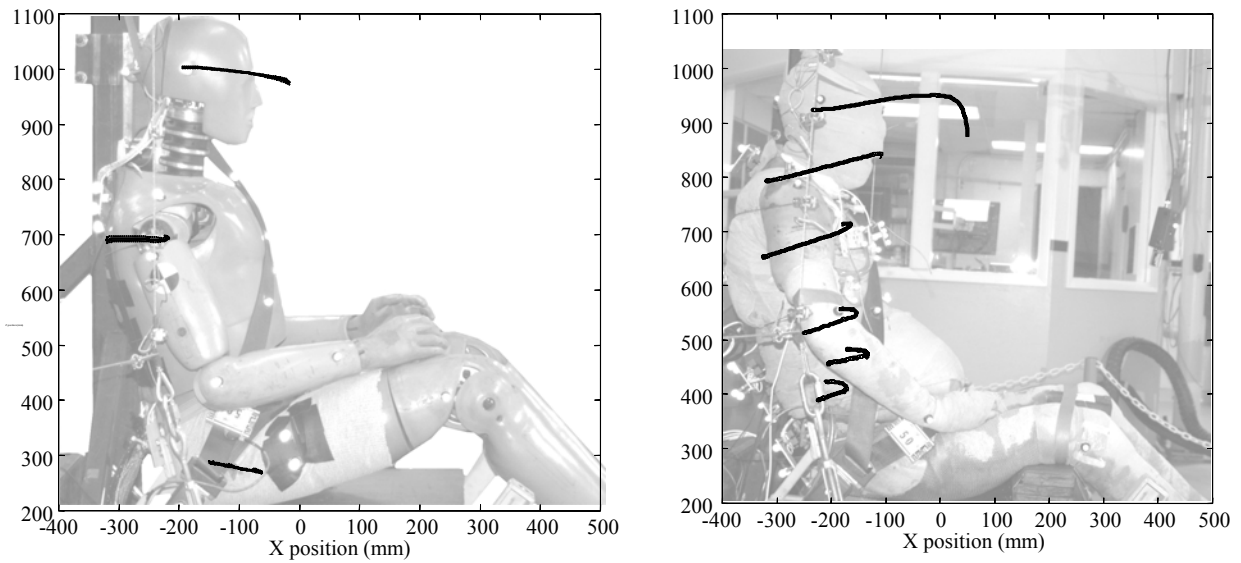


Figure 3. Comparison of the trajectories of head, spine and pelvis between the HIII 50<sup>th</sup> and a PMHS at low speed. (Note: ATD and PMHS contours are shown just for illustration purposes).

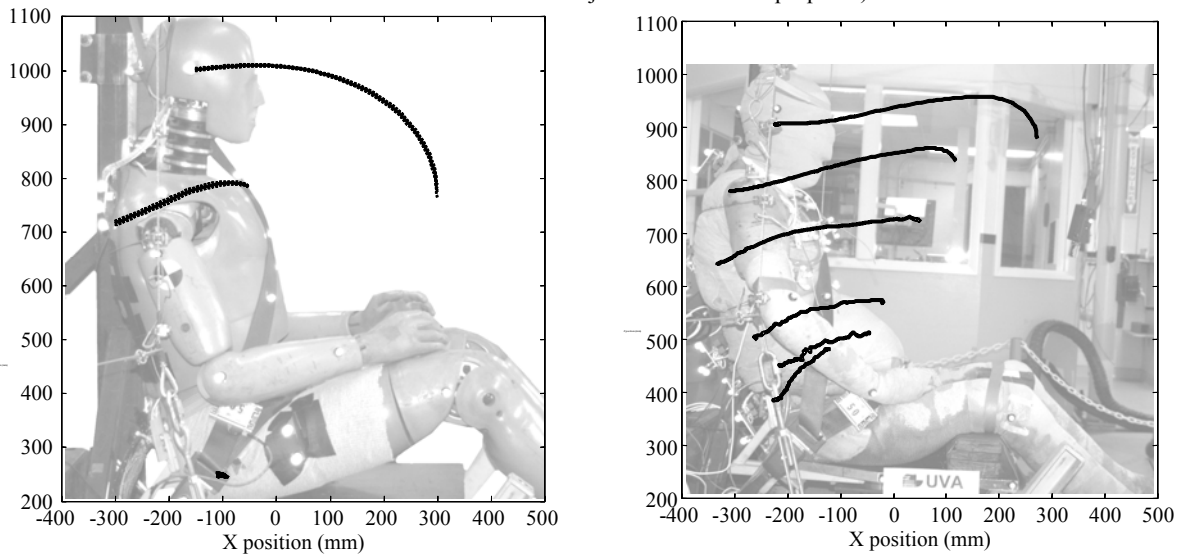


Figure 4. Comparison of the trajectories of head, spine and pelvis between the HIII 50<sup>th</sup> and a PMHS at high speed. (Note: ATD and PMHS contours are shown just for illustration purposes).

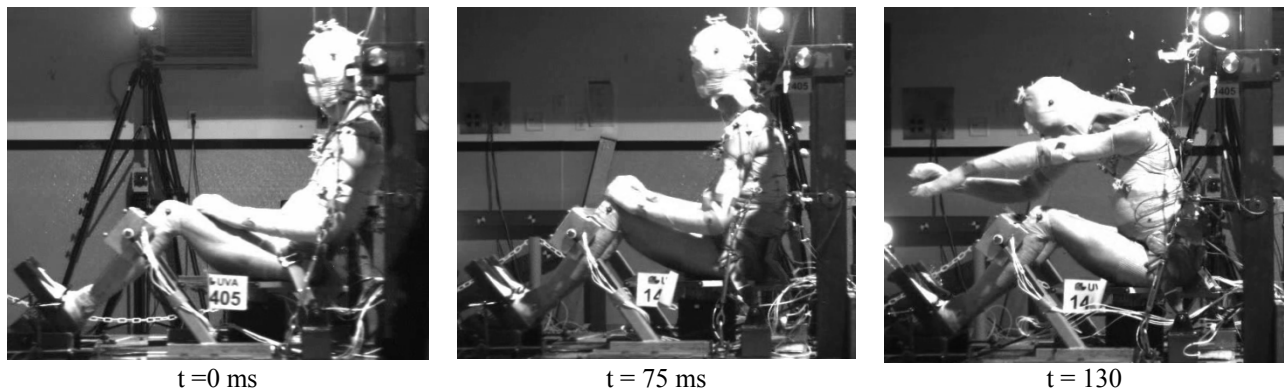


Figure 5. High speed video captures illustrating the kinematics of Test 1405 (high speed)

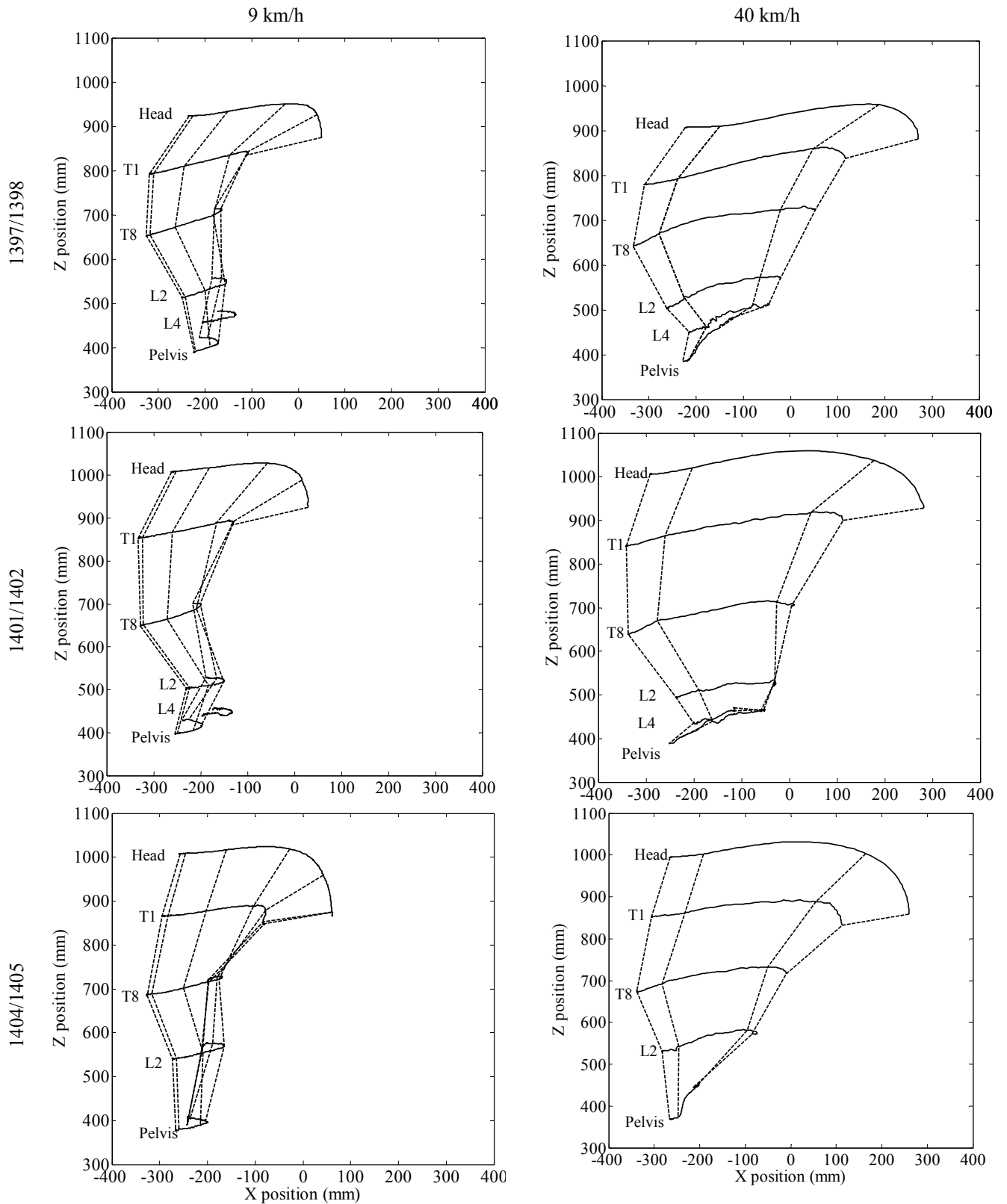


Figure 6. Comparison of the trajectories of the head and vertebral bodies XZ trajectories between low and high speed

### Estimated PMHS neck forces and moments

Peak ATD forces and moment at the upper neck load were directly obtained from the dummy load cell. Table 8 shows the mean and the standard deviation for the load measured by the ATD at low speed. The Injury Assessment Reference Values (IARV) at the OC/T1 junction have been added to Table 8 for comparison (Mertz et al., 2003). The combined axial force and moment neck injury criterion (Tension-Flexion),  $N_{TF}$ , was calculated according to the intercepts for the neck IARV proposed by Mertz et al. (2003) and the Federal Motor Vehicle Safety Standard No. 208 (FMVSS 208). The limit value in both procedures is  $N_{TF}=1$ . The value obtained in the low speed ATD tests (using both methods) was  $N_{TF}=0.06\pm 0.0$  (mean  $\pm$  standard deviation), substantially lower than the limit value established in the criteria.

The estimated values for the atlanto-occipital loads in the PMHS are included in Table 9. Axial forces are consistently greater in the PMHS. Two of the PMHS also exhibited larger shear force and flexion moment, though the differences in the estimation of the

moment are not significantly greater. Figure 7 shows the results obtained for the PMHS and compares them with the forces and moments registered by the ATD upper neck load cell at low speed.

Table 8. Peak ATD upper neck loads at low speed (Mean and standard deviation). IARV reference values (Mertz et al., 2003; FMVSS 208)

	Fx (N)	Fz (N)	My (Nm)
Mean	-236.6	80.3	20.4
Std. Dev	0.21	4.69	0.05
IARV	-3100	4170	190

Table 9. Peak PMHS atlanto-occipital loads at low speed.

	Fx (N)	Fz (N)	My (Nm)
1397	-220.2	407.6	13.4
1401	-326.4	370.1	24.3
1404	-378.7	474.6	28.3

The calculated PMHS head CG acceleration, PMHS head mass and PMHS head inertia were greater than the ATD, so this result is not unexpected.

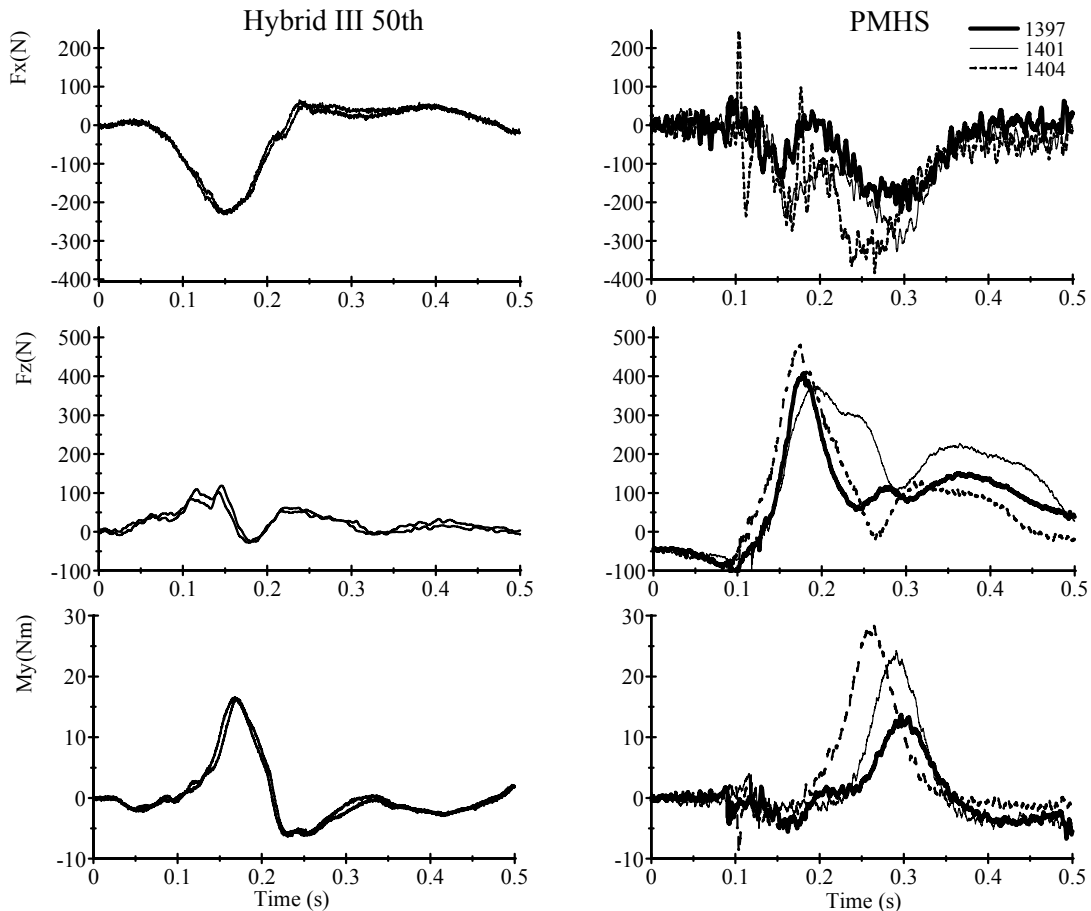


Figure 7. Comparison of neck loads between HIII 50<sup>th</sup> and PMHS at low speed.

Table 10 and Table 11 show the results obtained in the high speed tests, for the ATD and the PMHS respectively. The IARV defined for the OC/C1 junction of the ATD are included in Table 10 for comparison. At this speed, the assessment values of the combined neck tension-flexion mechanism were  $N_{TF}=0.27\pm0.02$  (FMVSS 208) and  $N_{TF}=0.28\pm0.01$  (IARV). In both cases, the calculated  $N_{TF}$  value was substantially lower than the limit value ( $N_{TF}=1$ ).

Table 10. Peak ATD upper neck loads at high speed (Mean and standard deviation). IARV reference values (Mertz et al., 2003; FMVSS 208)

	Fx (N)	Fz (N)	My (Nm)
Mean	-899.6	1534	73.1
Std. Dev	50.12	115.86	7.17
IARV	-3100	4170	190

Estimated forces and moments in the PMHS neck were higher than the measured ATD ones,

consistently for the three cadavers. The most important differences were found again in the value of the axial force. The comparison between the time histories of the neck loads is plotted in Figure 8.

Table 11. Peak PMHS atlanto-occipital loads at high speed.

	Fx (N)	Fz (N)	My (Nm)
1398	-1446.6	2696.0	89.43
1402	-1913.5	3909.3	102.35
1405	-2048.4	4170.4	99.7

In Test 1405, forces and moment curves were observed to oscillate as a consequence of the arm impacting the head of the PMHS at  $t=135$  ms. Accordingly, time history plots for this test were truncated at that time. The peak flexion moment reported in this paper corresponds to the instant prior to the start of oscillation. Since the peak moment was within the range of values obtained by the other two subjects in which this did not occur, it is reported here as the peak moment.

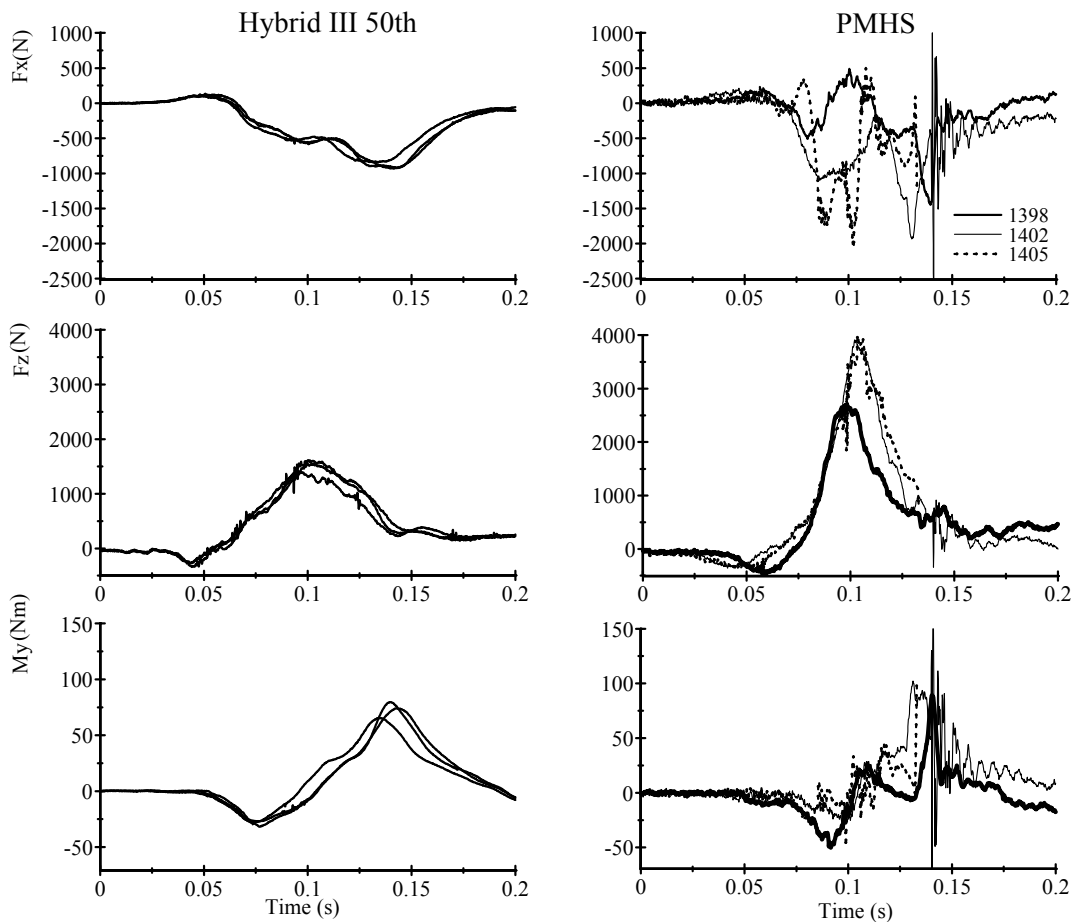


Figure 8. Comparison of neck loads between HIII 50<sup>th</sup> and PMHS at high speed.

## Injuries to the spine

PMHS 393 and PMHS 422 did not experience any spinal injuries as confirmed by the radiology examination and posterior autopsy. PMHS 462 exhibited a fracture of the anterior body of C4 (AIS 650230.2) involving disruption of the Anterior Longitudinal Ligament (ALL) (AIS 640284.1), avulsion fracture of the T1 left transverse process (AIS 650420.2) and fractures of the anterior vertebral body of T12 (AIS 650430.2) and spinous processes of T12 (AIS 650418.2) and L1 (AIS 650618.2), involving tearing of the ALL (AIS 650484.1).

## Belt forces

Belt forces at the upper shoulder and outer lap belt (buckle side) positions were measured in each test. Figure 9 and Figure 10 show the time history of the belt forces in the low speed and high speed tests respectively. At low speed, shoulder belt force peak was larger for the ATD ( $1518.3 \pm 135.4$  N, at 130 ms) than for any of the PMHS. However, the duration in time of the belt-occupant engagement was

longer for the PMHS and the area under the curve (mechanical impulse) was similar in both cases. Outer lap belt loads were substantially higher for the ATD ( $1235.7 \pm 128.5$  N, at 127 ms) again but in this case, ATD and PMHS engaged the belt for a comparable amount of time. Seat friction forces were greater in the PMHS, indicating a greater interaction of the subject with the seat (Figure 11, upper row). At high speed, ATD's peak shoulder belt force was  $4793.6 \pm 243.8$  N (at 110 ms) and peak lap belt was  $1092.16 \pm 37.7$  N (at 70 ms). In the PMHS tests, peak shoulder belt forces were 5509 N (PMHS 393) at 113 ms, 6328 N (PMHS 462) at 112 ms and 5204 N (PMHS 422) at 110 ms. Peak forces at the lap belt were 958 N at 112 ms (PMHS 393), 1954 N at 100 ms (PMHS 462) and 701 N at 109 ms (PMHS 422). Test 1402 (high speed, PMHS 462) resulted in an interval left femoral neck fracture that could explain why the lap belt peak force and the seat shear force are larger for this subject since the knee bolster was not restraining the forward motion of the pelvis any more.

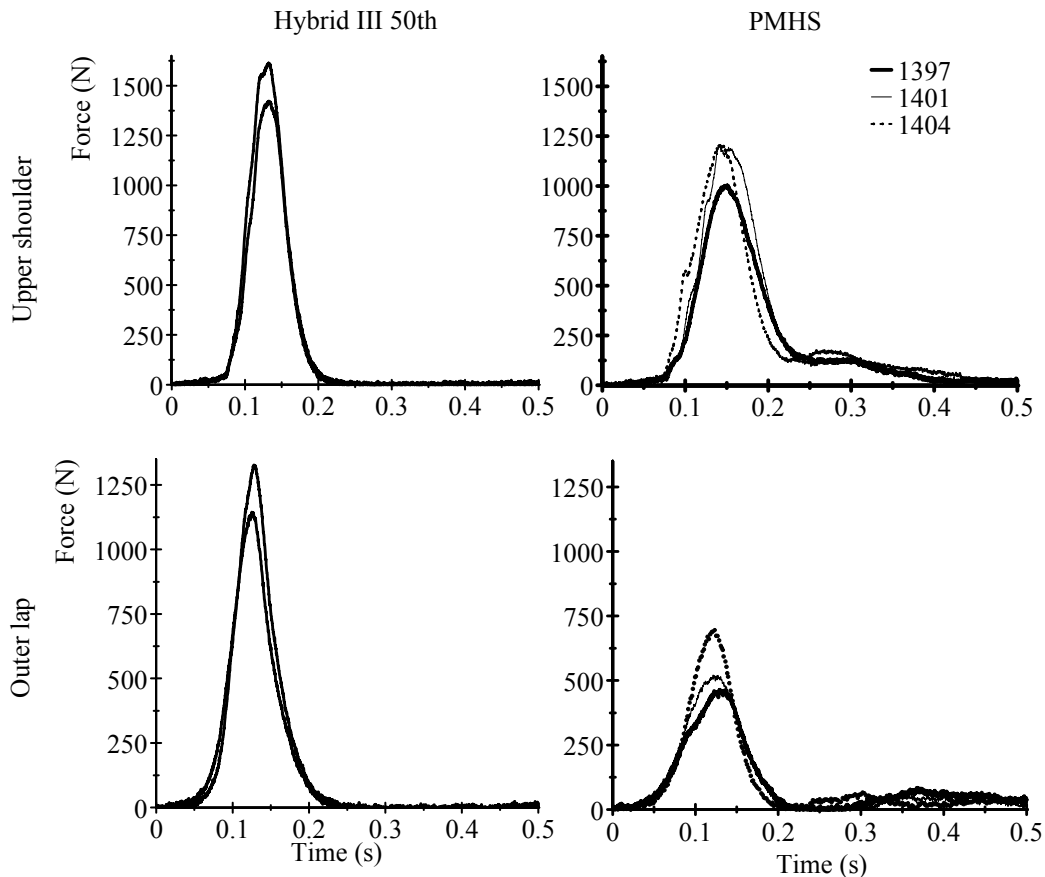


Figure 9. HIII 50<sup>th</sup> and PMHS belt forces at low speed

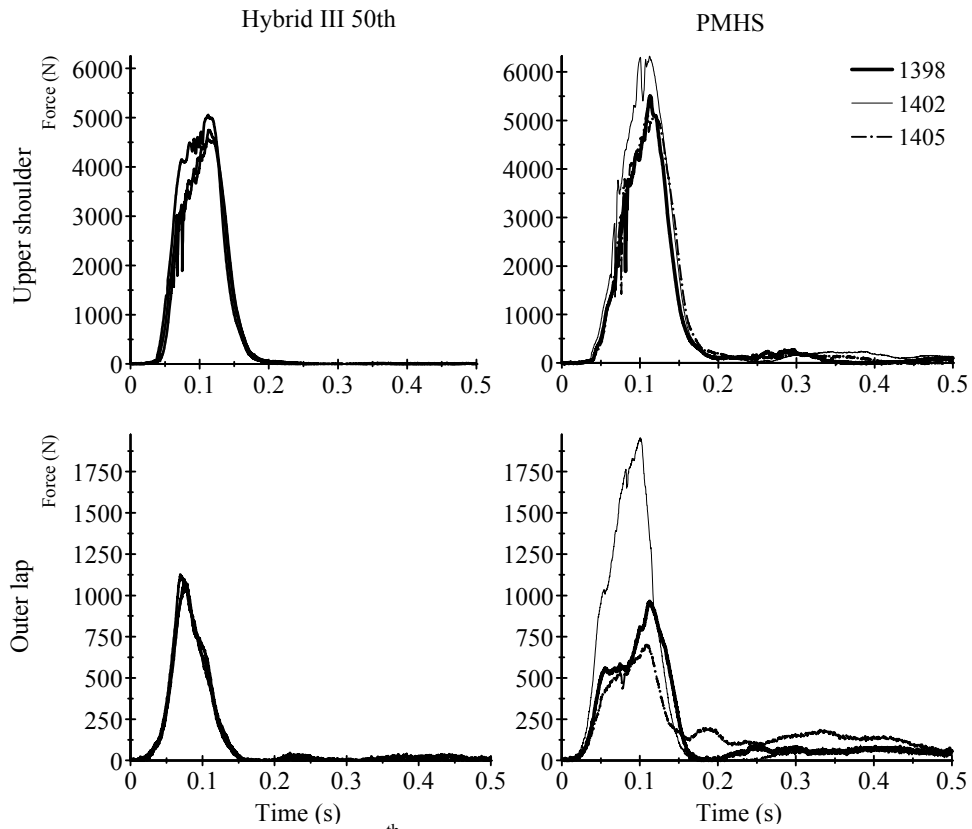


Figure 10. HIII 50<sup>th</sup> and PMHS belt forces at high speed

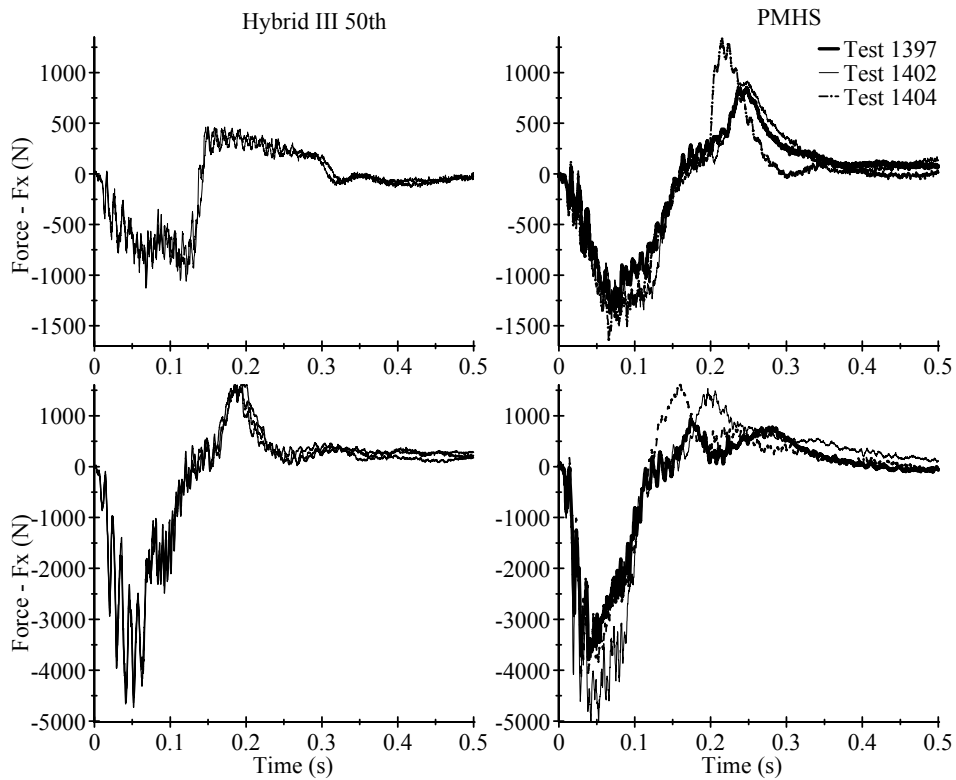


Figure 11. Comparison of seat shear forces ( $F_x$ ) between HIII 50<sup>th</sup> and PMHS at low (upper row) and high speed (lower row).

## DISCUSSION

This study analyzes a series of PMHS and ATD tests under two different loading conditions (low speed and high speed). The goals were to describe the spinal kinematics of the PMHS at both speeds and to investigate whether the neck loads predicted by the ATD were biofidelic in comparison with those estimated in the PMHS using inverse dynamics. The present paper is part of a broader scope study in which human volunteers were exposed to a similar crash pulse to the one used here at low speed. More information on this study can be found in Arbogast et al. (2009).

At low speed, the ATD produced greater shoulder and lap belt forces than the PMHS. As a result, peak shear force on the seat was greater for the three PMHS. This is compatible with the ATD exhibiting a greater forward displacement of the pelvis ( $87.0 \pm 0.5$  mm). Seacrist et al. (2010) showed similar results comparing the Hybrid III 6 YO with pediatric volunteers of an approximate anthropometry. PMHS head and upper spinal segments exhibited greater forward excursion than comparable ATD regions. According to Table 6, the time to reach maximum forward excursion increased from the pelvis to the head and Figure 6 shows how, except for T1, all the vertebrae as well as the pelvis were already in the rebound phase when the head is at its peak forward excursion. This result is consistent in the three PMHS. ATD trajectories did not reflect this behavior and the dummy tends to move forward almost synchronously. Displacements of the spine and pelvis are similar ( $102 \pm 1.8$  mm and  $87 \pm 0.5$  mm, respectively) and they occurred at about the same time ( $t = 138.5$  and  $t = 140$  ms), indicating almost a complete absence of rotation at the lumbar spine. Also, the occurrence of maximum forward displacements of the ATD spine and pelvis happens slightly after the time of maximum shoulder and belt lap forces ( $t = 130$  ms and  $t = 127$  ms). Figure 3 provides a qualitative assessment of this behavior comparing the ATD trajectories with one of the PMHS. However, these differences were expected since the Hybrid III 50<sup>th</sup> percentile was not designed to resemble the kinematics of the human body at such low speed.

Adult human volunteers included in the study by Arbogast et al. (2009) were 48.4% percentile in height and 47.9% percentile in weight in average. The same belt and belt geometry was used in both studies. Volunteers exhibited a mean peak force around 800 N at the shoulder portion of the belt and around 450 N at the lab pelt. Peak values happened

almost simultaneously at both locations (around 120 ms after the onset of sled acceleration). The differences with the PMHS results were minimal. In fact, if only the results from the larger volunteers (those closer to the size of the PMHS) are considered, peak values and timing are very close. Volunteers were asked to be in a relaxed state to minimize muscle influence. Very interestingly, volunteers and PMHS showed qualitatively the same behavior in their spinal kinematics: the head and upper spine levels lagging the lower levels in their forward displacement.

PMHS spinal kinematics showed a remarkable shift in behavior at high speed. Peak shoulder belt forces were comparable in magnitude between ATD and PMHS and they happened around the same time (approximately,  $t = 110$  ms). At the lap belt, PMHS exhibited smaller force (though there is variation in peak value among the PMHS and the shape of the force-time curve is more trapezoidal than the ATD one, see Figure 10). Maximum belt force was obtained earlier ( $t = 70$  ms) in the dummies than in the PMHS (approximately,  $t = 110$  ms) likely caused by the higher degree of coupling of the dummy pelvic structure. As discussed above, the femur fracture in Test 1402 caused the subject to generate unrealistically higher lap belt forces, since the knee bolster was not restraining the forward motion of the pelvis any more. Pre-test CT report of PMHS 422 manifested an advance degenerative disease of the hip joint which explains the occurrence of the femoral fracture for this subject. Contrarily to the low speed situation, maximum forward displacement was reached almost simultaneously by the head, all the spinal segments and the pelvis in the PMHS tests. Figure 6 provides a comparison between the low and high speed spinal deformation for the three PMHS. At high speed, the pelvis moved upward, probably as a consequence of the rotation around the lap belt, compressing the lower lumbar segments of the spine. On the contrary, upper segments were stretched due to the inertia of the head. At this speed, ATD exhibited greater differences in the timing between the head ( $t = 124.7$  ms) and spine ( $t = 130$  ms), on one side, and the pelvis ( $t = 71.3$  ms), on the other, to reach maximum forward excursion. The comparison with the timing of peak belt forces suggests that when the pelvis is stopped by the lap belt, the upper torso of the dummy started to rotate in the curvilinear trajectory depicted in Figure 4. The same figure shows that the forward excursion of the ATD pelvis was nearly completely impeded by the combination of the lap belt and the knee bolster. However, PMHS exhibited a considerable amount of pelvis motion

(both in X and Z directions) despite using the same restraints.

One of the goals of this study was to explore the influence of spinal flexibility on the values of upper neck loads. The results discussed above showed that for the same crash pulse, PMHS exhibited different kinematic features than ATD. The main difference relies on the fact that ATD segments (head, spine and pelvis) are more coupled than PMHS structures. ATD trajectories at low speed (with no knee bolster) showed that the whole dummy translated forward almost as a single rigid body and finally the neck allowed the head to rotate with respect to the torso. At high speed, the ATD pelvis is restrained completely by the lap belt and the knee bolster and this causes the upper torso to rotate and the neck to rotate with respect to the upper torso (Figure 3 and Figure 4). PMHS trajectories were more complex and different in nature. At low speed, lower spinal segments were already in rebound when the head was still reaching its maximum forward excursion. At high speed, lower segments of the spine appeared to be in compression and upper segments in extension. Moreover, the multi-segmented structure of the spine allowed for relative rotations between different spinal sections as showed in Figure 6. A fully quantitative characterization of these phenomena exceeded the scope of this paper, but it is needed to completely understand the nature of the spinal motion during a frontal impact.

Other studies have discussed the stiffness of the ATD spine as the cause of unrealistically high neck loads. Shaw et al. (2001) after completing a series of frontal sled tests using different restraints, showed the inability of the ATD to reproduce the lordotic curvature of the spine exhibited by PMHS. Using a human multibody model and locking the thoracic and lumbar joints and allowing the neck joints only to rotate (without translation), the study reported qualitative agreement between ATD and humans. Sherwood et al. (2003) after conducting a series of frontal sled tests with the Hybrid III 6YO and comparing the kinematics with previously published pediatric PMHS tests also identified the rigidity of the spine as a major cause of kinematic discrepancies between dummies and humans. To further explore the issue, they performed a set of MADYMO simulations modifying the spine of the dummy model by adding an additional joint to the thoracic spine. The study reported an improvement in the kinematics of the dummy (as compared to the pediatric PMHS) and also a significant reduction of upper and lower neck loads. Sherwood et al. (2003) also hypothesized that current pediatric ATD were overpredicting the

value of neck loads and that could explain why pediatric neck injuries were so rare in the field despite neck injury indices (such as  $N_{ij}$ ) being exceeded in the lab using ATD.

Since similar characteristics of thoracic rigidity were exhibited by adult ATD, the present study sought to compare upper neck loads between adult PMHS and adult ATD. It has been found that human axial and shear forces as well as flexion moments ( $F_x$ ,  $F_z$  and  $M_y$  according to SAE J211) were larger than those predicted by ATD. This is not surprising since a comparison of head accelerations showed greater values for the PMHS. Funk et al. (2009) reported qualitatively comparable results for the shear force and the flexion moment when comparing human volunteers and the Hybrid III head/neck responses to a soccer ball head impact. In this study, the axial force was larger in the dummy. It was attributed to the stiffer behavior of the Hybrid III neck at low levels of force. Yoganandan et al. (1989) discussed similar findings.

Mertz and Patrick (1971) proposed the equivalent moment at the OC-C1 junction as the best indicator of severity of neck flexion, finding that the shear and axial forces were not critical parameters in this regard. Culver et al. (1972) proposed a design for the Hybrid III neck focusing mainly in the flexion-extension characteristics discussed by Mertz and Patrick (1971). Mertz and Patrick (1971) also used an inverse dynamics method to estimate upper neck flexion loads in volunteers and cadavers. In the cadaver tests, the peak flexion moment at the atlanto-occipital joint was 189 Nm and the peak shear force was 1588 N. No ligamentous, disc or bone damage was found in this subject as noted from x-ray analysis. The study showed that an estimation of the PMHS moments at the occipital condyle junction produced higher values than those predicted by the ATD upper neck load cell. However, the performance corridor proposed by Mertz and Patrick (1971) was developed using volunteer data and therefore including muscle activity. The influence of neck musculature in neck forces and kinematics cannot be studied with the experimental work included in this paper. These studies can only be performed experimentally using volunteers and therefore at a sub-injurious acceleration level. Expanding on the work done by Arbogast et al. (2009), efforts are underway to estimate neck loads in the volunteers recruited in the former study. However, this is still an ongoing effort and no comparison is possible at this point. In a former study, Seeman et al. (1986) compared the response of the Hybrid III head-neck complex with human

volunteers subjected to a 15g deceleration, finding that the peak values for the acceleration of the head in X and Z were comparable between the ATD and the human. However, the study also reports differences in the XZ head trajectories that are similar to the ones presented in this paper.

As for the spinal injuries observed in the tests, the C4 anterior body fracture found in cadaver 462 could have been caused by the compression of the anterior region of the vertebral body during the flexion of the neck. Avulsion fractures of the vertebral processes could be also explained by the flexion of the spine.

There are a number of potential limitations to this study. The first one is that the PMHS neck loads estimation used here is correct only in absence of any other external forces applied to the head. If the head is contacted by any other object (including arms impacting the head and/or the chin contacting the torso of the subject), the additional load paths would introduce additional unknowns in the inverse dynamic equations and therefore the neck loads could not be determined. That situation was positively identified in Test 1405 and data were truncated to avoid confusion. The particular test setup needed for using a VICON system makes difficult to install high speed video cameras on the sled buck. Therefore the assessment of potential head contacts had to be done using two off board high speed video cameras. A conservative estimation is that there was no contact in any of the high speed tests (i.e Tests 1398, 1402 and 1405) up to at least 100 ms after trigger.

Also, the estimation of neck loads in the PMHS tests involved multiple challenges regarding data processing, such as data filtering and differentiation. When filtering was necessary, the cutoff frequency was selected after analyzing the frequency content of the original data calculating the Fast Fourier Transform of the data. The original (unfiltered) and the filtered curves were also inspected visually to assure that all the relevant information was contained in the filtered signal. According to this procedure, filtered dummy neck forces were filtered using a CFC 600 at low speed. More importantly, ARS data were initially filtered using a filter that would correspond to a CFC 30 (cutoff frequency of 50 Hz). Also, a CFC 60 filter was used in the calculation of the angular acceleration to remove the high frequency components introduced in the differentiation of the ARS signals. Similar difficulties and solutions were found and applied by Funk et al. (2009).

The initial position of the PMHS was chosen to be similar to the one used in the volunteer study

described in Arbogast et al. (2009). The positioning was based on three parameters: torso angle, femur angle and tibia angle, and PMHS and ATD were positioned initially according to the nominal values described in the methods of this study. The rest of the positioning parameters were chosen according to standard seating procedures as described in NHTSA (1990). However, it is not possible to achieve an ATD initial position that matches perfectly that of the PMHS. These differences in the initial positioning may influence the trajectories of the surrogates, and therefore they should be considered also as a limitation of the present study.

Finally, the accuracy of the 3D reconstruction methodology using the four markers arrays and obtaining the position and orientation in space of the bony structures has been discussed by Shaw et al. (2009). The standard deviation of the error in the optical system was found to be 1.4 mm in static conditions. Preliminary analysis on the compliance and vibration of the hardware limited the error to be less than 2 mm (Shaw et al., 2009). An estimation of the error under dynamic conditions is currently under development.

## CONCLUSION

A series of five Hybrid III 50<sup>th</sup> percentile and six PMHS frontal impact sled tests were performed using a 3D motion capture system. The objectives of the study were to characterize spinal kinematics during a frontal impact and to analyze the influence of spinal flexibility on upper neck loads at two different speeds. Results indicated a marked different behavior in spinal kinematics between the two different speeds and between ATD and PMHS. The multi-segmented structure of the human spine allowed for different motion patterns between the lower and upper spinal segments depending on the speed. Estimated upper neck loads (axial and shear force and flexion moment) at the atlanto-occipital joint of the PMHS produced larger values than those measured by the ATD.

## ACKNOWLEDGMENTS

The authors would like to acknowledge Takata Corporation, Japan for their collaboration and financial support for this study. The results presented in this report are the interpretation solely of the author(s) and are not necessarily the views of Takata Corporation.

## REFERENCES

Arbogast KB, Corejo RA, Kallan MJ, Winston FK, Durbin DR. Injuries to children in forward-facing

- child restraint systems in side impact crashes. Ann Proc Assoc Adv Automot Med Vol. 46, pp 213-230, 2002.
- Arbogast KB, Balasubramanian S, Seacrist T, Maltese MR, Garcia-Espana JF, Hopely T, Constans E, Lopez-Valdes FJ, Kent RW, Tanji H, Higuchi K. Comparison of Kinematic Responses of the Head and Spine for Children and Adults in Low-Speed Frontal Sled Tests. Stapp Car Crash Journal Vol. 53, pp 329-372, 2009.
- AAAM. The Abbreviated Injury Scale 2005. Association for the Advancement of Automotive Medicine, Barrington, IL, 2005.
- Beer FP, Johnston ER, Clausen WE (2004). Vector Mechanics for Engineers. Dynamics. 7<sup>th</sup> Edition. McGraw Hill, NY.
- Center for Applied Biomechanics. Protocol for the Handling of Biological Material. Version 4.3. University of Virginia, 2006.
- Culver CC, Neathery RF, Mertz HJ. Mechanical Necks with Humanlike Responses. SAE Paper No. 720959. In Hybrid III: The First Human-Like Crash Test Dummy, edited by Backaitis SH and Mertz HJ. Warrendale, 1994.
- Damon, AM. Characterizing the geometric and inertial properties of the adult human head for use in analysis and design (Master's Thesis). University of Virginia, Charlottesville, VA, 2009.
- Durbin D, Elliot M, Winston F. Belt positioning booster seats and reduction in risk of injury in motor vehicles. JAMA Vol. 289, No. 10, pp 2835-2840, 2003.
- FMVSS No. 208. Occupant crash protection. National Highway Traffic Safety Administration. Department of Transport.
- Funk JR, Cormier JM, Bain CE, Guzman H, Bonugli E. Validation and Application of a Methodology to Calculate Head Accelerations and Neck Loading in Soccer Ball Impacts. SAE International 2009-01-0251. Society of Automotive Engineers, 2009.
- Kinzel GL, Hall AS and Hillberry BM. Measurement of the total motion between two body segments – I. Analytical development. Journal of Biomechanics Vol. 5, pp 93-105, 1972.
- Lopez-Valdes FJ, Forman J, Kent RW, Bostrom O, Segui-Gomez M. A comparison between a child-size PMHS and the Hybrid III 6 YO in a sled frontal impact. Ann Proc Assoc Automot Med Vol 53, pp 237-246, 2009.
- Malott, A., C. Parenteau, S. Marigowda and K. Arbogast (2004). Sled test results using the Hybrid III 6 year olds: an evaluation of various restraints and crash configurations. SAE World Congress, Detroit, MI, Society of Automotive Engineers.
- Menon, R., Y. S. Ghata, S. Ridella, S. Roberts and F. K. Winston (2003). Evaluation of restraint type and performance tested with 3- and 6-year-old Hybrid III dummies at a range of speeds. SAE 2003 World Congress.
- Mertz HJ (1967). Kinematics and Kinetics of Whiplash. PhD Dissertation. Wayne State University, Detroit.
- Mertz HJ, Patrick LM. Strength and response of the human neck. Proceedings of the 15<sup>th</sup> Stapp Car Crash Conference, SAE paper 710855, pp 207-255, 1971.
- Mertz HJ, Irwin AL, Prasad P. Biomechanical and Scaling Bases for Frontal and Side Impact Injury Assessment Values. Stapp Car Crash Journal, Vol. 47 (October 2003), pp. 155-188.
- NHTSA (1990). Laboratory Indicant Test Procedure. New Car Assessment Program. U.S. Department of Transportation. National Highway Traffic Safety Administration. January 1, 1990.
- O'Flaherty, EJ Physiologically based models for bone-seeking elements. I. Rat Skeletal and Bone Growth. Toxicology and Applied Pharmacology 111: 299-312, 1991.
- SAE, SAE Information Report J1733 – Sign Convention for Vehicle Crash Testing. Society of Automotive Engineers, 1994.
- Seacrist T, Balasubramanian S, Maltese MR, Garcia-Espana JF, Lopez-Valdes FJ, Kent RW, Tanji H, Higuchi K, Arbogast KB. Kinematic Comparison Between Pediatric Human Volunteers and the Hybrid III 6-Year-Old Anthropomorphic Test Device. Annual Proc Assoc Adv Automot Med, 2010. Under Review.
- Seaman MR, Muzzy WH III, Lustick LS. Comparison of Human and Hybrid III Head and Neck Dynamic Response. Proceedings of the 30<sup>th</sup> Stapp Car Crash Conference. SAE paper 861892. Warrendale, 1986.

Shaw G, Parent D, Purtsezov S, Lessley D, Crandall J, Kent R, Guillemot H, Ridella S, Takhounts E, Martin P. Impact Response of Restrained PMHS in Frontal Sled Tests: Skeletal Deformation Patterns Under Seat Belt Loading. Stapp Car Crash Journal. Vol. 53, pp 1-48, 2009.

Shaw, C, Kent, R, Sieveka, E, Crandall, J. (2001) Spinal kinematics of restrained occupants in frontal impacts. IRCOBI Conference on the Biomechanics of Impact, Isle of Man.

Sherwood CP, Shaw CG, van Rooij L, Kent RW, Gupta PK, Crandall JR, Orzechowski KM, Eichelberger MR, Kallieris D. Prediction of cervical spine injury risk for the 6-year-old child in frontal crashes. Traffic Injury Prevention, 4:206-213, 2002.

Yoganandan N, Sances A Jr, Pintar F. Biomechanical Evaluation of the Axial Compressive Responses of the Human Cadaveric and Manikin Necks. Journal of Biomedical Engineering. Vol. 111: 250-255, 1989.

Zuckerbraun, BS, K. Morrison, B. Gaines, H.R. Ford, D.J. Hackam (2004) Effect of Age on 57 Cervical Spine Injuries in Children After Motor Vehicle Collisions: Effectiveness of Restraint Devices. J Pediatr Surg 39:483-486.

## ANNEX I. Verification of the dynamic equations

Calculating neck loads using inverse dynamics has been applied successfully in the past and the method does not need of any validation. However, as a check of the derivation of the inverse dynamics equations, the method was applied first to one of the ATD tests at both speeds. Figure 12 and Figure 14 show the comparison between the dummy measured upper neck loads and the predicted ones using the corresponding dynamic equations. Corrections proposed by SAE to account for the upper neck load cell geometry were implemented in the calculation (SAE, 1994).

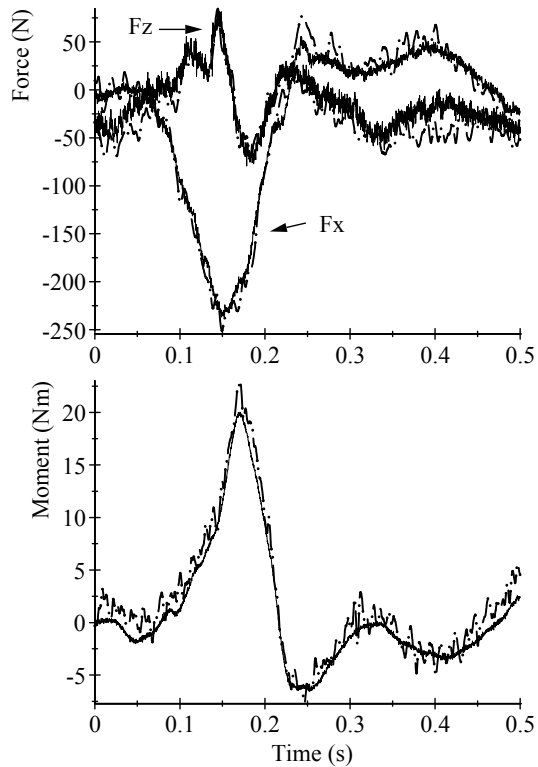


Figure 12. Comparison of measured (solid) and estimated (dashed) forces and moments at the dummy upper neck load cell in Test 1395 (low speed).

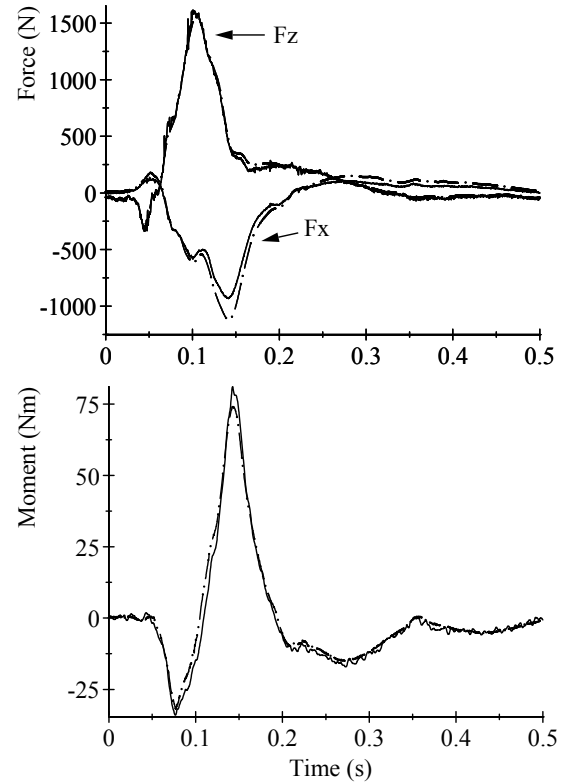


Figure 13. Comparison of measured (solid) and estimated (dashed) forces and moments at the dummy upper neck load cell in Test 1444 (high speed).

The comparison between the estimated and measured loads for the ATD showed a good agreement at both low and high speed. The same equations used here for the ATD were applied to the PMHS to obtain an estimation of the neck forces and moments.